Crystal growth and magnetic properties of Ln_4MGa_{12} (Ln = Dy–Er; M = Pd, Pt)

2007 J. Phys.: Condens. Matter 19 266224

(http://iopscience.iop.org/0953-8984/19/26/266224)

IOP PUBLISHING JOURNAL OF PHYSICS: CONDENSED MATTER

J. Phys.: Condens. Matter **19** (2007) 266224 (11pp) doi:10.1088/0953-8984/19/26/266224

Crystal growth and magnetic properties of Ln_4MGa_{12} (Ln = Dy–Er; M = Pd, Pt)

Jung Young Cho[1], Monica Moldovan[2], David P Young[2] and Julia Y Chan[1,3]

[1] Department of Chemistry, Louisiana State University, Baton Rouge, LA 70803, USA
[2] Department of Physics and Astronomy, Louisiana State University, Baton Rouge, LA 70803, USA

E-mail: jchan@lsu.edu

Received 1 March 2007, in final form 21 May 2007
Published 18 June 2007
Online at stacks.iop.org/JPhysCM/19/266224

Abstract

Single crystals of Ln_4MGa_{12} (Ln = Dy, Ho, Er; M = Pd, Pt) were synthesized by a flux technique using excess Ga and characterized by single crystal x-ray diffraction. Ln_4MGa_{12} (Ln = Dy, Ho, Er; M = Pd, Pt) crystallize in the cubic space group $Im\bar{3}m$ (no. 229) with lattice parameter $a \sim 8.5$ Å, $Z = 2$. Magnetic measurements show that Dy_4PdGa_{12} and Er_4PdGa_{12} are antiferromagnetic with transitions at $T_N = 10$ and 5.2 K, respectively, while Ho_4PdGa_{12} does not show any magnetic ordering down to 2 K. Ln_4PtGa_{12} (Ln = Dy, Ho, Er) order antiferromagnetically at $T_N = 9.8$, 3.6 and 5.1 K for Dy_4PtGa_{12}, Ho_4PtGa_{12} and Er_4PtGa_{12}, respectively. The electrical resistivity data show metallic behaviour. Large positive magnetoresistance is shown for each compound, up to 900% at 3 K and 9 T for the Ho_4PtGa_{12} analogue.

1. Introduction

Ternary intermetallic compounds consisting of RE–M–Ga (RE = rare earth; M = transition metal) are interesting to study due to the wide range of structural features and physical properties they exhibit [1–7]. Our interest lies in finding new rare earth-based ternary intermetallic compounds, which exhibit exotic physical properties such as heavy fermion behaviour [8, 9] and large magnetoresistance.

Recently, An_4PdGa_{12} (An = U, Np, Pu) have been reported as new heavy fermion compounds [10]. Each compound exhibits a Sommerfeld coefficient $\gamma \sim 330, 450$ and 900 mJ mol^{-1} K^{-2} for the U, Np and Pu compounds, respectively. U_4PdGa_{12} also shows an antiferromagnetic transition at $T_N \sim 43$ K. The Np and Pu analogues, however, do not order magnetically down to 2 K. Compounds having the stoichiometry of 4:1:12 crystallize in

[3] Author to whom any correspondence should be addressed.

the cubic $Im\bar{3}m$ (no. 229) space group and have been described as a redistributed homologue of the $U_4Re_7Si_6$ structure type [11] or a superstructure of the $AuCu_3$ type. Polycrystalline Ln_4MGa_{12} (Ln = Ho, Tm; M = Ni, Pd) show metallic behaviour [12]. Single crystals of $Ln_4FeGa_6Ge_6$ (Ln = Sm, Tb), grown using molten gallium as a flux are isostructural to Y_4PdGa_{12} [13]. Transport measurements for the isostructural $Ln_4FeGa_6Ge_6$ (Ln = Sm, Tb) also show metallic behaviour [13]. $Sm_4FeGa_6Ge_6$ does not magnetically order down to 2 K, while the Tb analogue orders antiferromagnetically at $T_N = 13$ K [13]. In our study with the Ln–M–Ga (Ln = lanthanide; M = Pd, Pt) system, we have been able to synthesize Tb_4MGa_{12} (M = Pd, Pt) which order antiferromagnetically at 16 and 12 K, respectively [2]. With early lanthanides, however, we were not able to synthesize the 4:1:12 analogues under our conditions.

Large positive magnetoresistance has also been found in other Ln–Pd–Ga compounds. The transport and magnetic properties in these materials are strongly coupled, and large positive magnetoresistance is often observed. $SmPd_2Ga_2$ ($ThCr_2Si_2$-type), which is composed of layers of isolated Sm atoms and layers of $PdGa_4$ edge-sharing tetrahedra alternating along the *c*-axis, orders ferromagnetically at 5 K. The low temperature (2 K) field-dependent resistivity shows large positive magnetoresistance over 100% at 9 T [14]. The low temperature (2 K) magnetoresistance of Ce_2PdGa_{10}, a layered structure consisting of alternating Ce–Ga bilayers and Ga–Pd layers, increases by over 200% at 9 T [6]. In this paper, we discuss the crystal growth, transport, magnetoresistance and magnetic properties of Ln_4MGa_{12} (Ln = Dy, Ho, Er; M = Pd, Pt).

2. Experimental details

2.1. Synthesis

The samples were synthesized from lanthanide (Dy, Ho, Er) pieces, palladium or platinum powder and gallium shot, which were obtained from Alfa Aesar, all with purities greater than 99.9%. The lanthanide (Dy, Ho, Er) pieces were combined with palladium or platinum powder and gallium pellets in a molar ratio of 1:1:20. The samples were then placed in alumina crucibles, sealed in a fused silica tube, gradually heated (200 °C h^{-1}) to 1150 °C for 7 h, and slow cooled (15 °C h^{-1}) to 530 °C, at which point the excess flux was removed via centrifugation. The synthesis yielded metallic single crystals which ranged in size from 0.2 to 0.5 cm^3. The crystals were stable in air.

2.2. Single crystal x-ray diffraction

Single crystal fragments of an average size of ∼0.08 mm × 0.08 mm × 0.08 mm were mechanically extracted, placed on a glass fibre and mounted on the goniometer of a Nonius Kappa CCD diffractometer equipped with Mo Kα radiation ($\lambda = 0.71073$ Å). The data were then corrected, reduced and scaled using the SHELXL [15] software package. The structures were solved using Tb_4PtGa_{12} as a structural model. The structure consists of four atomic positions in which the lanthanide (Ln) occupies the 8c (1/4, 1/4, 1/4) site, the transition metal (Pd, Pt) occupies the 2a (0, 0, 0) site, Ga1 the 12d (1/4, 0, 1/2) site and Ga2 the 12e (y, 0, 0; where $y \sim 0.2900$) site. Additional data collection and crystallographic parameters are presented in table 1. Atomic positions and thermal displacement parameters are given in table 2. Selected interatomic distances are listed in table 3.

2.3. Physical property measurements

Transport and magnetic measurements were performed on single crystals of Ln_4MGa_{12} (Ln = Dy, Ho, Er; M = Pd, Pt). The electrical resistance was measured by the standard four-

Table 1. Crystallographic parameters.

Crystal data						
Formula	Dy_4PdGa_{12}	Dy_4PtGa_{12}	Ho_4PdGa_{12}	Ho_4PtGa_{12}	Er_4PdGa_{12}	Er_4PtGa_{12}
a (Å)	8.5700(5)	8.5630(7)	8.5490(7)	8.5400(6)	8.5300(7)	8.5350(9)
V (Å^3)	629.42(6)	627.88(9)	624.81(9)	622.84(8)	620.65(9)	621.74(11)
Z	2	2	2	2	2	2
Crystal system	Cubic	Cubic	Cubic	Cubic	Cubic	Cubic
Space group	$Im\bar{3}m$	$Im\bar{3}m$	$Im\bar{3}m$	$Im\bar{3}m$	$Im\bar{3}m$	$Im\bar{3}m$
Mosaicity (deg)	0.445(6)	0.462(7)	0.445(2)	0.485(7)	0.494(9)	0.623(2)
θ range (deg)	3.36–29.84	3.36–29.87	3.37–29.92	3.37–29.96	3.38–30.00	3.38–29.98
μ (mm^{-1})	49.938	59.756	51.715	61.653	53.608	63.306
Data collection						
Measured reflections	305	297	301	288	276	252
Independent reflections	113	110	114	112	114	108
Reflections with $I > 2\sigma(I)$	111	108	107	109	108	104
R_{int}	0.0452	0.0566	0.0410	0.0348	0.0507	0.0430
h	$-11 \rightarrow 12$	$-11 \rightarrow 11$	$-11 \rightarrow 12$	$-11 \rightarrow 12$	$-11 \rightarrow 12$	$-11 \rightarrow 11$
k	$-8 \rightarrow 8$	$-8 \rightarrow 8$	$-8 \rightarrow 8$	$-8 \rightarrow 8$	$-8 \rightarrow 8$	$-8 \rightarrow 8$
l	$-7 \rightarrow 7$	$-7 \rightarrow 7$	$-7 \rightarrow 7$	$-7 \rightarrow 7$	$-7 \rightarrow 7$	$-7 \rightarrow 7$
Refinement						
R_1 $[F^2 > 2\sigma\ (F^2)]$[a]	0.0277	0.0338	0.0305	0.0414	0.0284	0.0268
wR^2 (F^2)[b]	0.0639	0.0720	0.0582	0.0952	0.0715	0.0642
Reflections	113	110	114	112	114	108
Parameters	10	10	10	10	10	10
$\Delta\rho_{\text{max}}$ (e Å^{-3})	2.082	3.404	2.383	4.808	2.499	2.102
$\Delta\rho_{\text{min}}$ (e Å^{-3})	−2.172	−1.764	−2.229	−4.797	−1.889	−1.641

[a] $R_1 = \sum ||F_o| - |F_c|| / \sum |F_o|$.
[b] $wR_2 = [\sum[w(F_o^2 - F_c^2)] / \sum[w(F_o^2)^2]]^{1/2}$.

probe AC technique at 27 Hz with a current of 1 mA. Pt wires of diameter 1 mil (0.001 in, 0.0254 mm) were attached to the sample with silver epoxy. The magnetic susceptibility measurements were performed using a Quantum Design physical property measurement system. The samples were zero-field-cooled (ZFC) to 2 K and then warmed to room temperature in a constant DC field of 1000 G (0.1 T).

3. Results and discussion

3.1. Synthesis and structure

Single crystals of Ln_4MGa_{12} (Ln = Dy, Ho, Er; M = Pd, Pt) were synthesized using molten gallium as a flux. Similar to $Ln_4FeGa_6Ge_6$ (Ln = Sm, Tb) [13], we find that a shorter isothermal ($\leqslant$3 days) step for the growth of these phases leads to the formation of the cubic phase. In addition, upon the substitution of early rare earths such as cerium and praseodymium in the synthesis at 500 °C, we find that Ln_2PdGa_{10} (Ln = Ce, Pr) is formed [6].

Dy_4PdGa_{12} consists of $PdGa_6$ octahedra corner-shared with the Ga framework and $DyGa_3$ cuboctahedra as shown in figure 1. The lattice parameters of Ln_4MGa_{12} (Ln = Dy, Ho, Er; M = Pd, Pt) decrease linearly with the decrease in the rare earth atomic radii due to lanthanide contraction. The lattice parameters for the Ln_4PdGa_{12} (Ln = Dy, Ho, Er) are in agreement with those reported from polycrystalline data for Ln_4PdGa_{12} (Ln = Gd–Tm, Lu) [12]. Six Ga1

Table 2. Atomic positions and thermal parameters.

Atom	Wyckoff position	x	y	z	U_{eq} (Å^2)[a]
		Dy_4PdGa_{12}			
Dy	8c	1/4	1/4	1/4	0.0032(4)
Pd	2a	0	0	0	0.0055(6)
Ga1	12d	1/4	0	1/2	0.0047(5)
Ga2	12e	0.2952(2)	0	0	0.0050(5)
		Dy_4PtGa_{12}			
Dy	8c	1/4	1/4	1/4	0.0059(4)
Pt	2a	0	0	0	0.0069(5)
Ga1	12d	1/4	0	1/2	0.0075(6)
Ga2	12e	0.2962(3)	0	0	0.0075(6)
		Ho_4PdGa_{12}			
Ho	8c	1/4	1/4	1/4	0.0037(4)
Pd	2a	0	0	0	0.0064(6)
Ga1	12d	1/4	0	1/2	0.0049(5)
Ga2	12e	0.2952(2)	0	0	0.0057(4)
		Ho_4PtGa_{12}			
Ho	8c	1/4	1/4	1/4	0.0021(6)
Pt	2a	0	0	0	0.0039(6)
Ga1	12d	1/4	0	1/2	0.0027(7)
Ga2	12e	0.2958(3)	0	0	0.0036(6)
		Er_4PdGa_{12}			
Er	8c	1/4	1/4	1/4	0.0038(4)
Pd	2a	0	0	0	0.0061(7)
Ga1	12d	1/4	0	1/2	0.0047(5)
Ga2	12e	0.2953(3)	0	0	0.0054(5)
		Er_4PtGa_{12}			
Er	8c	1/4	1/4	1/4	0.0092(4)
Pt	2a	0	0	0	0.0104(5)
Ga1	12d	1/4	0	1/2	0.0095(5)
Ga2	12e	0.2959(3)	0	0	0.0106(5)

[a] U_{eq} is defined as one-third of the trace of the orthogonalized U_{ij} tensor.

atoms and six Ga2 atoms are coordinated to each lanthanide atom. The interatomic distances in the cuboctahedra of Ln_4MGa_{12} (Ln = Dy, Ho, Er; M = Pd, Pt) are listed in table 3. They scale well with the summation of the values for the atomic radii of Ga (1.26 Å) and Dy (1.59 Å), Ho (1.58 Å) or Er (1.57 Å) [16]. The Ln–Ga1 interatomic distances in Ln_4MGa_{12} (Ln = Dy, Ho, Er; M = Pd, Pt) are in agreement with those found in $LnGa_6$ (La–Yb) [17] and range from 3.188 to 3.307 Å.

Similarly, the Ln–Ga2 interatomic distances are also in agreement with those found in $LnGa_6$ (La–Yb), which range from 3.077 to 3.138 Å [17]. The Ga–Ga interatomic distances in Ln_4MGa_{12} (Ln = Dy, Ho, Er; M = Pd, Pt) are slightly larger than those found in the cuboctahedra of $LnGa_3$ (La–Tm) [18], which range from 2.101 to 2.830 Å. The ratio of Ln–Ga(1) to Ln–Ga(2) in each cuboctahedron is ∼1, indicating that the cuboctahedra are highly symmetrical.

Table 3. Selected interatomic distances (Å).

	M = Pd	M = Pt
	Dy_4MGa_{12}	
Dy–Ga1 (×6)	3.02995(18)	3.0275(2)
Dy–Ga2 (×6)	3.0547(3)	3.0533(4)
M–Ga2 (×6)	2.530(2)	2.537(3)
	Ho_4MGa_{12}	
Ho–Ga1 (×6)	3.0225(2)	3.0193(2)
Ho–Ga2 (×6)	3.0471(4)	3.0445(4)
M–Ga2 (×6)	2.524(2)	2.526(3)
	Er_4MGa_{12}	
Er-Ga1 (×6)	3.0158(2)	3.0176(3)
Er-Ga2 (×6)	3.0404(4)	3.0429(4)
M–Ga2 (×6)	2.519(2)	2.526(2)

The transition metal environment in Ln_4MGa_{12} (Ln = Dy, Ho, Er; M = Pd, Pt) is six-coordinate to gallium and forms MGa_6 octahedra. The interatomic distances are listed in table 3. The (Pd, Pt)–Ga interatomic distances, which range from 2.519(2) to 2.537(3) Å, are smaller than those reported for the $PdGa_6$ octahedra of Ce_8PdGa_{24} (2.633–2.927 Å) [19, 20]. The (Pd, Pt)–Ga interatomic distance in the octahedra of Tb_4PdGa_{12} and Tb_4PtGa_{12} is 2.5444(3) and 2.5341(3) Å, respectively [2]. The (Pd, Pt)–Ga interatomic distances in Ln_4MGa_{12} (Ln = Dy, Ho, Er; M = Pd, Pt) are also comparable to those found in CePdGa and TbPdGa, which range from 2.5609 to 2.6350 Å [21].

3.2. Physical properties

Figure 2 shows the temperature-dependent magnetic susceptibility of single crystals of Ln_4PdGa_{12} (Ln = Dy, Ho, Er) measured at an applied field of 0.1 T. Dy_4PdGa_{12} shows magnetic ordering at 10 K. Fitting the inverse susceptibility data to a Curie–Weiss fit of the form $\chi(T) = C/(T - \theta)$, an effective moment of 10.53 μ_B/Dy atom was obtained, and a Weiss constant, $\theta = -27.28$ K, indicates antiferromagnetic correlations. No magnetic ordering is observed down to 2 K for Ho_4PdGa_{12} (open squares). The magnetic susceptibility data for Er_4PdGa_{12} (closed triangles) show an antiferromagnetic transition at $T_N = 5.2$ K. An effective moment of 9.47 μ_B/Er atom is obtained from the inverse magnetic susceptibility data with $\theta = -9.57$ K. The experimental moments for Dy_4PdGa_{12} and Er_4PdGa_{12} are close to the calculated values of 10.63 and 9.59 μ_B for Dy^{3+} and Er^{3+}, indicating that the magnetism in these materials is solely due to the trivalent rare earth atoms. The experimental magnetic moment of 10.48 μ_B and $\theta = -17.36$ K obtained for paramagnetic Ho_4PdGa_{12} is also close to the full Hund's value for Ho^{3+} of 10.60 μ_B. The negative Weiss constant in the Ho compound suggests that antiferromagnetic correlations exist between the local moments in this system, and it could quite possibly display long-range order below 2 K.

Figure 3 shows the field-dependent isothermal magnetization of Ln_4PdGa_{12} (Ln = Dy, Ho, Er) measured at a constant temperature of 3 K. The magnetization for Dy_4PdGa_{12} (closed circles) increases linearly with field, which is typical for an antiferromagnet. No long-range magnetic ordering for Ho_4PdGa_{12} was observed down to 2 K, and the magnetization versus field displays typical paramagnetic behaviour and does not saturate up to 9 T. The

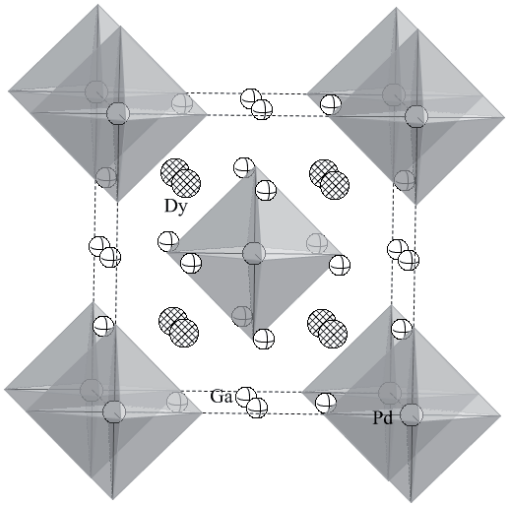

Figure 1. The crystal structure of Dy_4PdGa_{12} is shown along the *c*-axis. Dysprosium, palladium and gallium atoms are represented as white (hollow hatched spheres), grey and white (hollow equatorial spheres) circles, respectively. The dashed lines represent the unit cell.

(This figure is in colour only in the electronic version)

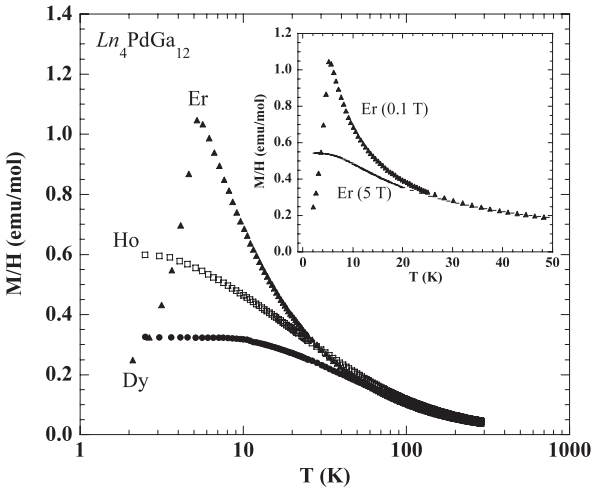

Figure 2. Zero-cooled magnetic susceptibility as a function of temperature of Ln_4PdGa_{12} (Ln = Dy, Ho, Er) at 0.1 T is shown. The inset shows the magnetic susceptibility of Er_4PdGa_{12} at 0.1 and 5 T.

magnetization of Er_4PdGa_{12} (closed triangles), however, is very different from the other two. At low fields (<1000 G) the magnetization increases more or less linearly with field. Above 5000 G, however, the magnetization increases sharply in a metamagnetic transition whose midpoint is ∼1 T. Above 2 T, the magnetization displays paramagnetic behaviour out to 9 T. Field-dependent neutron scattering measurements will be necessary to correctly determine the magnetic structure in this material, but the data suggest that the metamagnetism is associated with a spin–flip transition. Below T_N (figure 2), the magnetization in the Er sample decreases

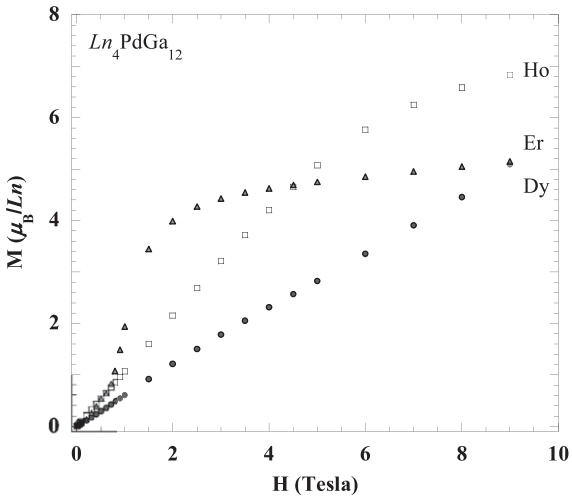

Figure 3. The magnetization as a function of field of Ln_4PdGa_{12} (Ln = Dy, Ho, Er) at 3 K.

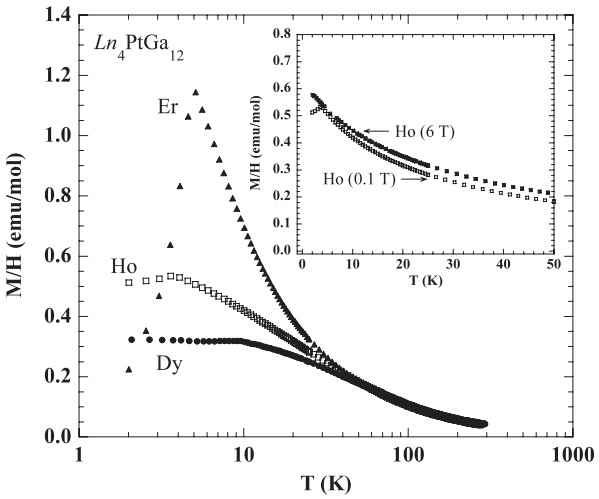

Figure 4. Zero-cooled magnetic susceptibility as a function of temperature of Ln_4PtGa_{12} (Ln = Dy, Ho, Er) at 0.1 T. The inset shows magnetic susceptibility of Ho_4PtGa_{12} at 0.1 and 6 T.

rapidly and extrapolates to zero at zero temperature, suggesting the axis of the spins are well aligned parallel and antiparallel to the applied field (the field here being applied along one of the cubic axis directions.) As the field is increased above 5000 G, the spin system flips (discontinuously) to lower the energy. The transition in figure 3 is fairly broad (∼1.5 T), since the measurement is performed at finite temperature close to T_N. A temperature sweep of the susceptibility at 5 T (dashed curve, figure 2, inset) clearly shows that the parallel susceptibility is completely suppressed below T_N.

The temperature-dependent magnetic susceptibility of Ln_4PtGa_{12} (Ln = Dy, Ho, Er) is shown in figure 4 measured at 0.1 T. We find the magnetic moment of 10.54, 9.94 and 9.50 μ_B for Dy_4PtGa_{12} (closed circles), Ho_4PtGa_{12} (open squares) and Er_4PtGa_{12} (closed triangles). All three compounds order antiferromagnetically with ordering temperatures of 9.8, 3.6 and 5.1 K,

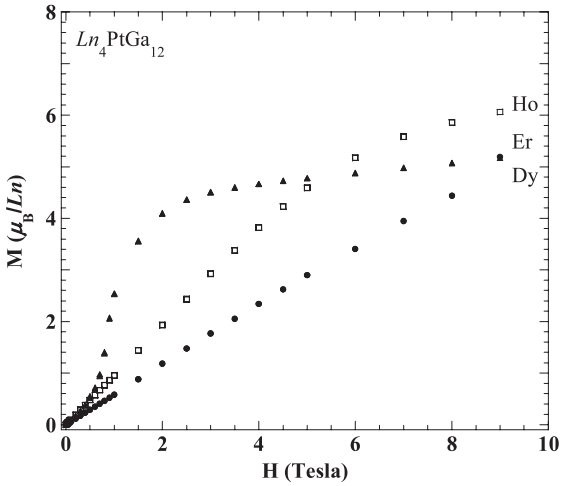

Figure 5. The magnetization as a function of field of Ln_4PdGa_{12} (Ln = Dy, Ho, Er) at 3 K.

Table 4. Magnetic properties of Ln_4MGa_{12} (Ln = Dy, Ho, Er; M = Pd, Pt). (Abbreviations: T_N, Néel temperature; AFM, antiferromagnetic; MM, metamagnetic.)

	C	θ (K)	μ_{calc} (μ_B)	μ_{eff} (μ_B)	Fit range (K)	Ordering T_N (K)
Dy_4PdGa_{12}	13.858	−27.28	10.63	10.53	50–250	AFM 10
Dy_4PtGa_{12}	13.873	−27.89	10.63	10.54	50–250	AFM 9.8
Ho_4PdGa_{12}	13.728	−17.36	10.60	10.48	50–250	N/A
Ho_4PtGa_{12}	12.339	−15.44	10.60	9.94	50–250	AFM 3.6
Er_4PdGa_{12}	11.216	−9.57	9.59	9.47	50–250	AFM 5.2; MM, 1T
Er_4PtGa_{12}	11.275	−10.47	9.59	9.50	50–250	AFM 5.1; MM, 1T

respectively. The effective magnetic moments obtained for the three Pt analogues are also close to the expected values for Dy^{3+} (10.63 μ_B), Ho^{3+} (10.60 μ_B) and Er^{3+} (9.59 μ_B). In addition, we have measured the temperature-dependent magnetization of Ho_4PtGa_{12} and found that the ordering temperature disappears at 6 T. The AF behaviour is destroyed and paramagnetism is recovered at high field.

The field-dependent magnetization of Ln_4PtGa_{12} (Ln = Dy, Ho, Er) measured at 3 K is shown in figure 5. Similar to the Pd analogue, the magnetization of Dy_4PtGa_{12} (closed circles) increases linearly with field and is typical of antiferromagnetic systems. The magnetization of Ho_4PtGa_{12} shows linearity up to 5 T and does not saturate up to 9 T. The magnetization of Er_4PtGa_{12} is very similar to the Pd material and shows a metamagnetic transition, again with a midpoint around 1 T. A summary of the magnetic properties of Ln_4MGa_{12} (Ln = Dy, Ho, Er; M = Pd, Pt) is given in table 4.

The electrical resistivities as a function of temperature of single crystals of Ln_4PdGa_{12} (Ln = Dy, Ho, Er) are shown in figure 6. The samples show metallic behaviour ($d\rho/dT > 0$) with residual resistivity ratio (RRR) values of 4.7, 3.3 and 3.1 for Dy_4PdGa_{12}, Ho_4PdGa_{12} and Er_4PdGa_{12}, respectively. The inset of figure 6 shows a blow-up of the low temperature resistivity data. Kinks in the resistivity are consistent with a decrease in the spin-disorder scattering at temperatures coinciding with magnetic ordering. As shown in figure 7, the magnetoresistance ($MR\% = (\rho_H - \rho_0)/\rho_0 \times 100$) data as a function of field of Ln_4PdGa_{12} (Ln = Dy, Ho, Er) show positive values of 45%, 10% and 16% for Dy_4PdGa_{12}, Ho_4PdGa_{12} and

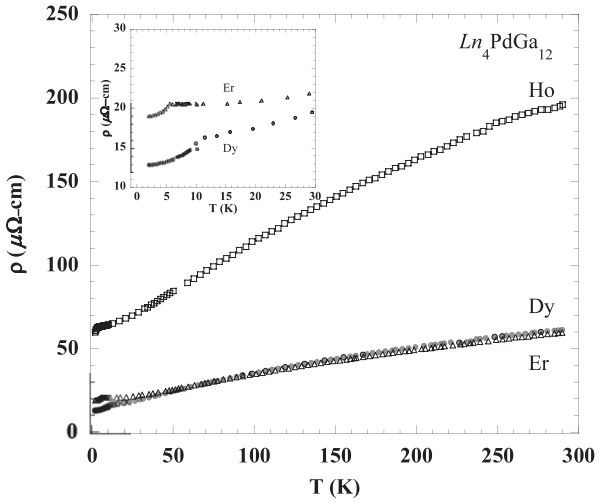

Figure 6. The electrical resistivity of single crystals of Ln_4PdGa_{12} (Ln = Dy, Ho, Er).

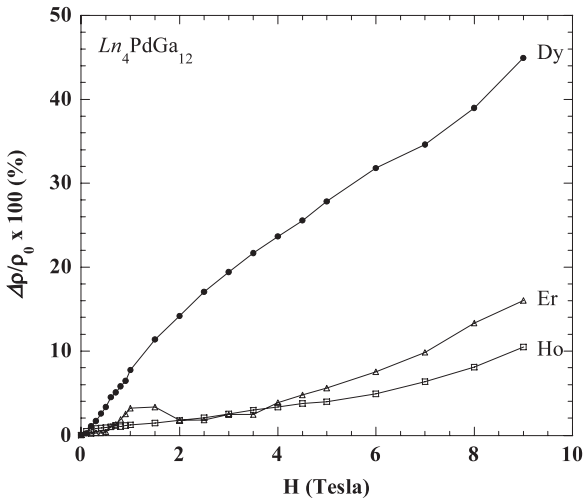

Figure 7. The magnetoresistance of Ln_4PdGa_{12} (Ln = Dy, Ho, Er) as a function of field at 3 K.

Er_4PdGa_{12}, respectively, at 3 K and 9 T. The MR of the Er sample (open triangles) increases as H^2 until ∼1 T, where there is a sharp peak in the MR, coinciding with the metamagnetic transition. Since the MR data were taken close to T_N, spin fluctuations in the AFM state probably play a role in the resistivity scattering processes. These are eliminated at higher fields above the metamagnetic transition. Another possible explanation for the MR behaviour would be field-dependent changes in the Fermi surface topology. As such, this material is a good candidate for de Haas–van Alphen measurements, which we will pursue in the near future. At fields above the metamagnetic transition, the MR is again $\sim H^2$.

Figure 8 shows the electrical resistivity as a function of temperature of single crystals of Ln_4PtGa_{12} (Ln = Dy, Ho, Er). These materials are also metallic ($d\rho/dT > 0$) with RRR values of 4.2, 8.6 and 4.4 for Dy_4PtGa_{12}, Ho_4PtGa_{12} and Er_4PtGa_{12}, respectively. A blow-up (figure 8 inset) of the low temperature resistivity reveals kinks in the data, concomitant with the Néel

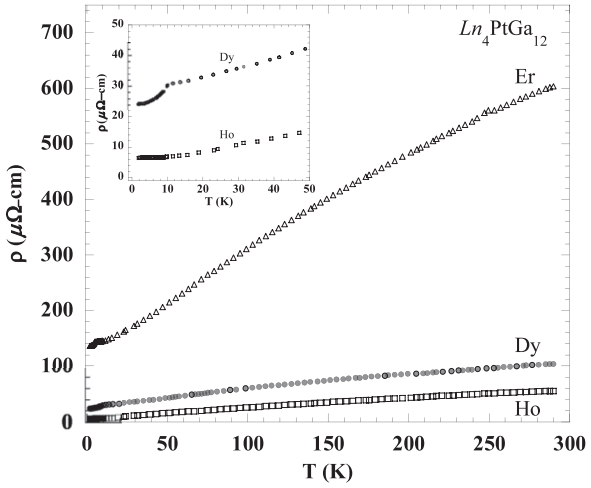

Figure 8. The electrical resistivity of single crystals of Ln_4PtGa_{12} (Ln = Dy, Ho, Er).

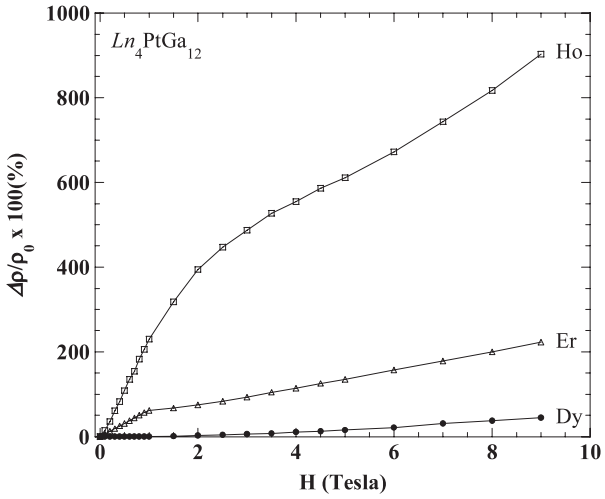

Figure 9. The magnetoresistance of Ln_4PtGa_{12} (Ln = Dy, Ho, Er) as a function of field at 3 K.

temperatures. The magnetoresistance of Ln_4PtGa_{12} (Ln = Dy, Ho, Er) is shown in figure 9. The Er compound (open triangles) shows a behaviour similar to its Pd counterpart. A kink at the metamagnetic transition (∼1 T) is observed, although the data do not strictly follow H^2 behaviour either below or above the transition. Interestingly, large positive MR of Ln_4PtGa_{12} (Ln = Dy, Ho, Er) with 50%, 220% and 900% at 3 K and 9 T are observed for Dy_4PtGa_{12}, Er_4PtGa_{12} and Ho_4PtGa_{12}, respectively. Large positive magnetoresistance has been reported in other Ln–M–Ga compounds, such as $YbCo_2Ga_8$ [22] (200% at 50 kOe $\mu\Omega^{-1}$ cm^{-1} and 2 K) and $SmPd_2Ga_2$ [14] (100% at 9 T and 2 K), respectively. Compared to figure 7, the data in figure 9 suggest that the MR in these two sets of materials depends sensitively upon the Pd or Pt d-levels near the Fermi surface. The very large MR in the Ho sample is particularly interesting. Furthermore, there are subtle features in its data set, such as the soft peak in its susceptibility (figure 4) and the inflection point in its MR data near 5.5 T (figure 9) that suggest that crystal

electric field (CEF) effects may be important in the analysis of its physical properties. As future work, electronic structure calculations and field-dependent specific heat measurements can help clarify these open questions.

Acknowledgments

We would like to acknowledge useful discussions with Ilya Vekhter and Willa M Williams. JYC gratefully acknowledges support from the NSF-DMR no. 02-37664 and Alfred P Sloan Foundation. DPY acknowledges NSF-DMR no. 04-49022.

References

[1] Thomas E L, Millican J M, Okudzeto E K and Chan J Y 2006 *Comment. Inorg. Chem.* **27** 1
[2] Williams W M, Moldovan M, Young D P and Chan J Y 2005 *J. Solid State Chem.* **178** 52
[3] Wawryk R, Henkie Z, Cichorek T, Geibel C and Steglich F 2002 *Phys. Status Solidi* b **232** R4
[4] Wawryk R, Stepien-Damm J, Henkie Z, Cichorek T and Steglich F 2004 *J. Phys.: Condens. Matter* **16** 5427
[5] Opahle I and Oppeneer P M 2003 *Phys. Rev. Lett.* **90** 157001
[6] Millican J N, Macaluso R T, Young D P, Moldovan M and Chan J Y 2004 *J. Solid State Chem.* **177** 4695
[7] Grin Y N, Yarmolyuk Y P and Gradyshevsky E I 1979 *Kristallografiya* **24** 242
[8] Fisk Z, Hess D W, Pethick C J, Pines D, Smith J L, Thompson J D and Willis J O 1988 *Science* **239** 33
[9] Stewart G R 1984 *Rev. Mod. Phys.* **56** 755
[10] Jardin R, Colineau E, Wastin F, Rebizant J and Sanchez J P 2006 *Physica* B **378–380** 1031
[11] Akselrud L G, Jarmoljuk J P and Gladyshevskij E I 1978 *Dopov Akad. Nauk* **4** 359
[12] Vasilenko L O, Noga A S, Grin Y N, Koterlin M D and Yarmolyuk Y P 1988 *Russ. Metall.* **5** 216
[13] Zhuravleva M A, Wang X P, Schultz A J, Bakas T and Kanatzidis M G 2002 *Inorg. Chem.* **41** 6056
[14] Williams W M, Moldovan M, Young D P and Chan J Y 2003 *Inorg. Chem.* **42** 7315
[15] Sheldrick G M 1997 *SHELXL97* University of Göttingen, Germany
[16] Shannon R D 1976 *Acta Crystallogr.* A **32** 751
[17] Pelleg J, Kimmel G and Dayan D 1981 *J. Less-Common Met.* **81** 33
[18] Cirafici S and Franceschi E 1981 *J. Less-Common Met.* **77** 269
[19] Gordon R A and DiSalvo F J 1996 *Z. Naturf.* B **51** 52
[20] Gordon R A, Jones C D W, Alexander M J and DiSalvo F J 1996 *Physica* B **225** 23
[21] Penc B, Szytula J, Hernandez-Velasco J and Zygmunt A 2003 *J. Magn. Magn. Mater.* **256** 373
[22] Fritsch V, Bobev S, Moreno N O, Fisk Z, Thompson J D and Sarrao J L 2004 *Phys. Rev.* B **70** 052410